4

Suspension mode control

4.1 Introduction

The previous chapter describes an electromagnet control scheme which is capable of producing an electromagnetic force actuation that is dominantly linear and stable. This chapter now develops the sophisticated suspension mode control strategy proposed in Chapter 1 and employs the aforementioned force actuator to provide a non-contacting suspension system.

The suspension mode controller is a component of the multi-electromagnet vehicle control system described in Chapter 5. However, it is first developed and tested using a single electromagnet suspension configuration in order to simplify the design and verification stages.

The description of the development of the suspension mode control system is partitioned into six sections. First, the functional requirements of the suspension are identified. A sophisticated suspension control strategy is then proposed, and the strategy is developed by analysing the proposed closed-loop suspension system and synthesising each system component. The characteristic behaviour of the passive lateral electromagnet guidance motion is then briefly analysed. Finally, some simulated and experimental responses are presented and discussed, and conclusions are then drawn on the performance of the proposed system.

4.2 Functional requirements

The primary functional requirement for an electromagnetic suspension system is to follow the general guideway profile whilst providing a quality of ride consistent with

passenger comfort.[61] This requirement calls for a control system with two conflicting aims. Guideway following requires the suspension to be effectively coupled to the track, whilst ride comfort considerations require the suspension to be isolated from track irregularities.

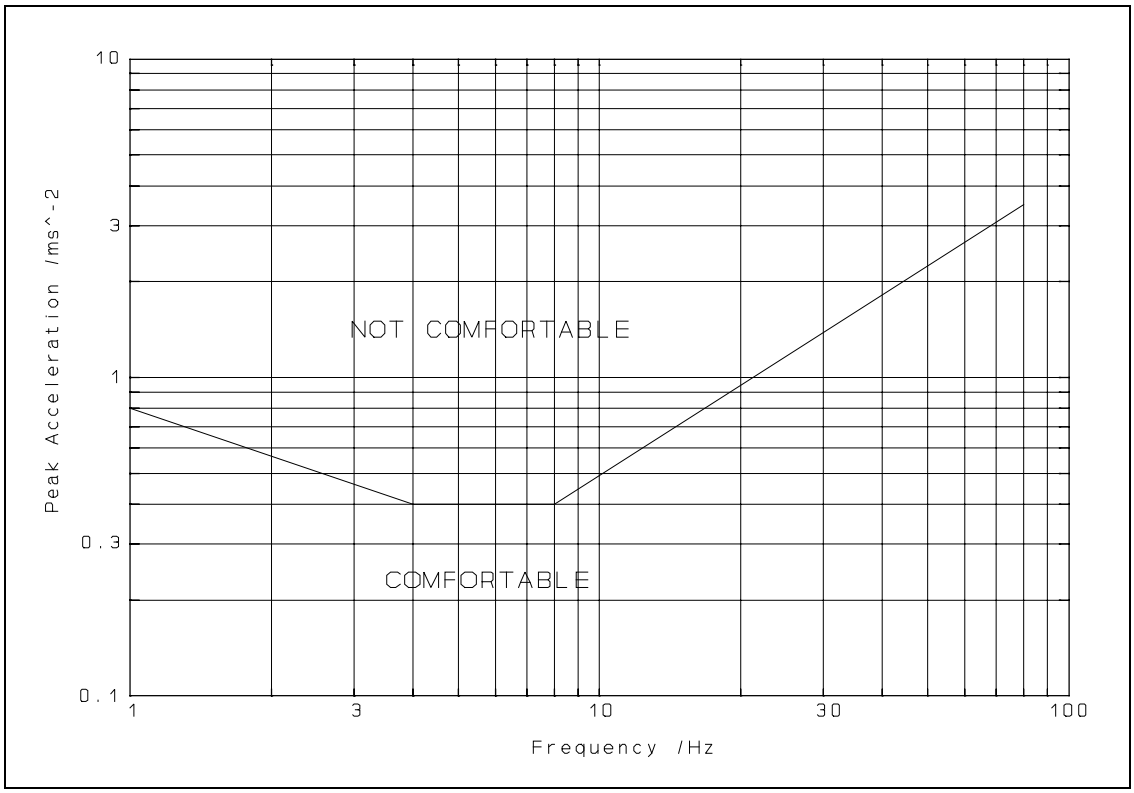

Figure 4.1 ISO reduced comfort boundary (for a 1 hour exposure)

Passenger ride comfort is a subjective measure which depends on the individual in question. However, it has been recorded that irrespective of the individual in question, the human body is particularly sensitive to vibration over a frequency range of about 1-20 Hz. In 1974 the International Standards Organisation (ISO) produced a guide[62] which incorporated a specification for vertical acceleration versus frequency corresponding to the threshold between human comfort and discomfort. For urban transport applications, the ISO's one hour exposure characteristic is appropriate (see Figure 4.1) for which the peak acceleration limit is 0.4 m/s^2 over the frequency range 4-8 Hz.

For an electromagnetic suspension with no conventional secondary suspension (ie. no springs and dampers), suspension travel is limited to the operating air gap range of the electromagnet. This suspension configuration therefore requires a stiff track, with a deflection restricted to about 50% of the normal operating air gap deviation.

The ride comfort analysis for vehicle suspensions is generally performed by considering the track roughness.[63] However, since the guideway for the proposed low-speed system consists of stiff, smooth track sections, which are joined together, a ride quality specification in terms of a worst case track joint misalignment is more convenient. A suspension designed to accommodate significant track steps is desirable since it permits cost savings in track production and maintenance.[64] Therefore, after allowing for operational air gap deviations, it is desirable for the suspension to accommodate a worst-case track step size of 50% of the nominal operating air gap deviation. The suspension acceleration when negotiating such a track step must be within the ISO comfort specification (see Figure 4.1). To improve upon existing light rail systems, which have a typical peak vertical acceleration[65] level of 0.4 m/s^2, a design target of 0.2 m/s^2 is considered desirable for the proposed electromagnetic suspension system.

In addition to the track oriented functional requirements discussed so far, the suspension system must reject disturbance forces due to variations in the weight of the payload, wind gusts, and vertical forces generated by the linear inductance motor[66] which propels the vehicle along its guideway. Accommodation of disturbance forces of 30-50% of the maximum vehicle weight is typically required.[67] Therefore, the design target for the proposed system is for a transient air gap deflection of 30-50% of the operating gap deviation, for a disturbance force equal to 30-50% of the maximum suspended weight. In addition, there must be no steady-state air gap deflection due to disturbance forces in order to maximise the available air gap deviation.

Having identified the functional requirements of the electromagnetic suspension, the suspension system structure proposed in Chapter 1 is now examined and developed.

4.3 Suspension control strategy

The vehicle suspension control system structure proposed in Chapter 1 is applied to a single electromagnet suspension as illustrated in Figure 4.2. The suspension strategy involves the calculation of the absolute track position, which is then suitably processed to provide an absolute position reference demand for the high stiffness electromagnet position controller. The force actuation demand from the position controller is then fed to the electromagnet force controller which is described in Chapter 3. Strategies for designing the electromagnet position controller and the guideway following algorithm are outlined next.

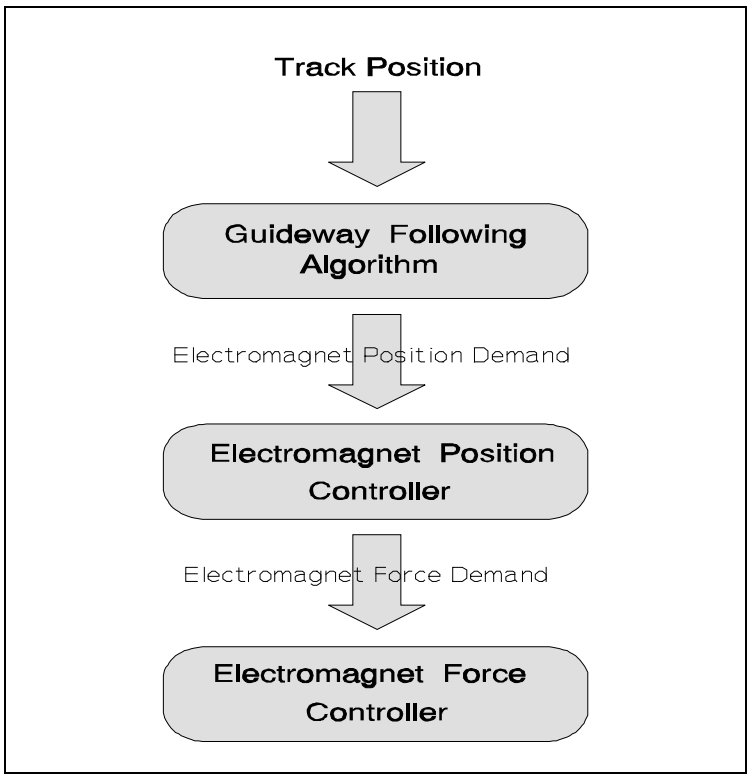

Figure 4.2 Suspension control system hierarchy

The electromagnet position controller is the heart of the suspension system. It must control the absolute position of the suspension with zero steady-state error, and it must also resist disturbance forces and accommodate load variations. The minimum properties required of the position controller therefore include stiffness, damping, and position error integral action.

Implementing this control system structure is complicated by the lack of a physical link between the electromagnet and an absolute datum. Measurement of the absolute position of the electromagnet is therefore not readily achievable, but absolute acceleration can be cost-effectively measured using a standard industrial accelerometer. The acceleration measurement must be integrated to give the absolute velocity, which must in turn be integrated to give the absolute position. Pure integrators would suffer from drift problems due to erroneous offsets, so a high-pass filter must augment each integrator. Since acceleration is measured, the position controller can incorporate acceleration feedback to assist in the control task. The proposed state-vector used for feedback thus consists of position, and integral of position error, together with output velocity and acceleration.

The absolute position of the track can be calculated using the absolute electromagnet position and the electromagnet air gap measured using an industrial non-contacting

displacement sensor. The function of the guideway following algorithm is to receive the track position and to transform it to a suspension position reference signal which avoids contact with the track and which provides a comfortable ride quality. The design of the guideway following algorithm depends on several factors. The most important ones are the operational air gap deviation, the vehicle speed, the size of track discontinuities, and finally, the parameters of track gradient entries and exits.

Since acceleration is the second derivative of displacement, a guideway following algorithm consisting of a second-order low-pass filter can be used to limit acceleration for a given size of track discontinuity on an otherwise flat guideway. However, Pollard and Williams[68] showed that the use of solely linear control algorithms presents considerable difficulties and operational limitations when designing for gradient entries and exits. It is therefore envisaged that the use of techniques such as matched-filtering[69] could provide better performance than traditional linear filtering. For example, a matched-filter could be programmed with the functions used to define the gradient entries and exits. These may consist of straight track segments, smoothly curved sections, or a combination of both. Having identified the underlying guideway profile curvature, linear filtering may then be suitable for rejecting discontinuities superimposed on the curved profile.

If a guideway profile is encountered which cannot be comfortably negotiated, the guideway following algorithm must attempt to limit the air gap deviation in order to prevent the mechanical air gap limit stops from being reached. Similar techniques may also be required for lateral guidance of the suspension.

The design of suitable guideway following algorithms, for both vertical and lateral motion, represents a large research project in itself and is peripheral to the main objective of this research work. Therefore, for the experimental research system, the use of a second-order linear filter is proposed for the vertical motion guideway following algorithm. In order to reduce the cost and complexity of experimental system hardware, the lateral motion is not actively controlled.

The logical arrangement of the suspension system is outlined in Figure 4.3, and the configuration of the proposed suspension control system is illustrated in Figure 4.4. Table 4.1 lists the control system variables and parameters.

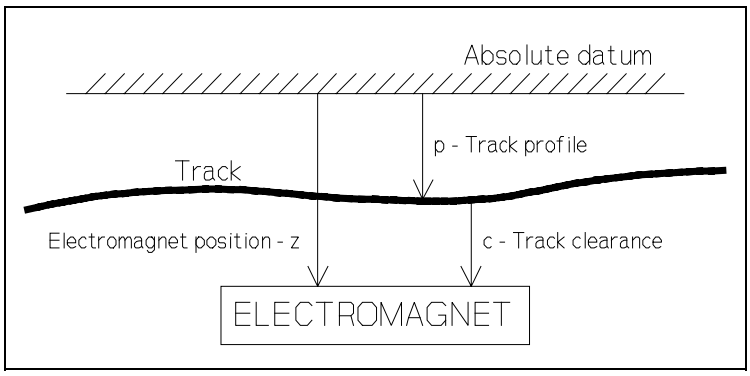

Figure 4.3 Logical arrangement of the suspension system

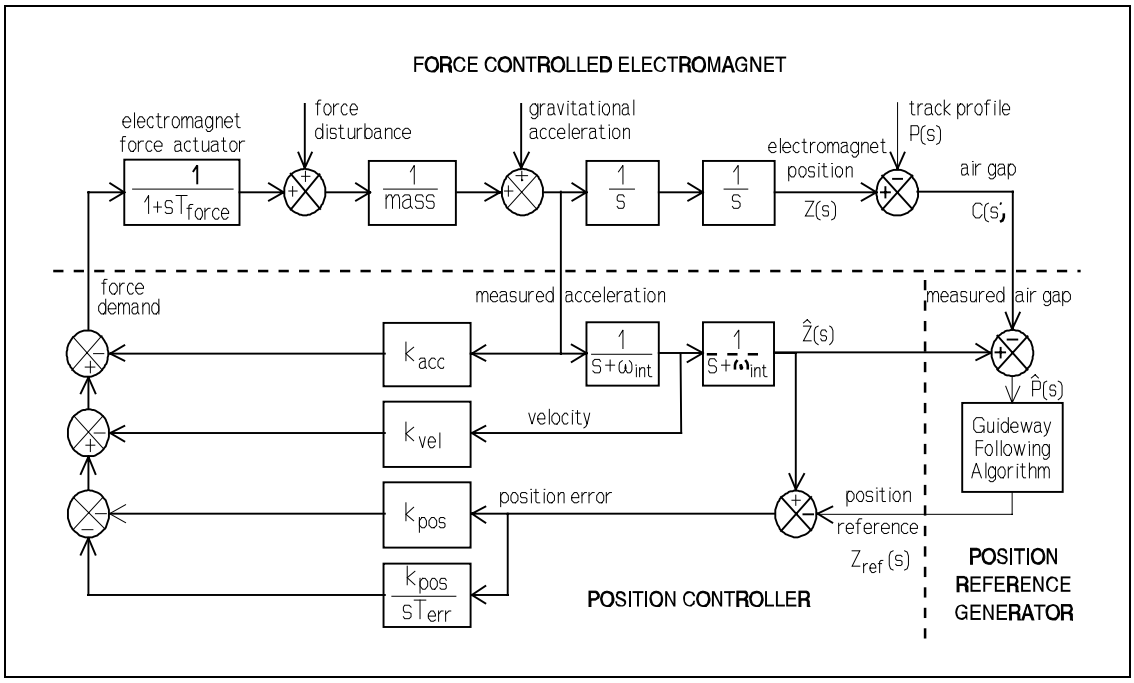

Figure 4.4 Suspension control system configuration

Inspection of Figure 4.4 shows that the position error signal consists of a component of both the absolute position signal and the position signal relative to the track. The proportion and frequency spectrum of each component is determined by the guideway following algorithm. The coupling of the electromagnet suspension to the track is therefore dominated by the guideway following algorithm. In order to be able to isolate the suspension design procedure from the guideway dynamics, a sufficient margin must be provided between the natural frequency of the track and the suspension to track coupling frequency.

The analysis and synthesis of the position controller, the guideway following filter, and the state integration filters are described next.

Table 4.1 Suspension control system nomenclature

Identifier	Variable / Parameter
$Z(s)$	Electromagnet absolute position (ˆ - calculated position)
$P(s)$	Track absolute position (ˆ - calculated position)
$C(s)$	Electromagnet to track air gap
$Z_{ref}(s)$	Position controller reference signal
$F_{demand}(s)$	Position controller force demand
$F_{disturb}(s)$	Disturbance force input
k_{acc}	Acceleration feedback gain (virtual mass)
k_{vel}	Velocity feedback gain (damping)
k_{pos}	Position feedback gain (stiffness)
T_{err}	Position error integral action time constant
ω_{int}	State integration filter corner frequency
T_{force}	Electromagnet force actuation time constant
m	Suspended mass

4.4 Synthesis of the suspension control system

The proposed suspension control system is developed by analysing the closed-loop system and then synthesising each system component. The position, velocity and acceleration feedback gains are designed first, then an acceptable force actuation bandwidth is determined. Next, a suitable error integral action time constant is chosen. Finally, the guideway following algorithm is designed, and an acceptable cut-off frequency for the state integration filters is determined. The development is concluded by identifying a simplified transfer function which characterises the suspension system response.

4.4.1 Position control transfer function

In order to be able to design the position controller and the guideway following algorithm on a largely independent basis, two restrictions must be imposed on the guideway algorithm. Firstly, the guideway algorithm must pass the track position signal for frequencies below ω_{int} so that the bandwidth of the position error signal extends down to dc. Also, the guideway following algorithm must have a gain not exceeding unity at all frequencies so that the position error feedback gain is determined solely by k_{pos}. In practice, these are fundamental requirements of all guideway following algorithms and therefore they do not impose any operational restrictions.

The Laplace transform of the full position control law illustrated in Figure 4.4 is given by:

$$F_{demand}(s) = -\left(k_{pos} + \frac{k_{pos}}{sT_{err}}\right)\left(\frac{s^2 Z(s)}{(s+\omega_{int})^2} - Z_{ref}(s)\right) - k_{vel}\frac{s^2 Z(s)}{(s+\omega_{int})} - k_{acc} s^2 Z(s) \qquad \textbf{4.1}$$

The acceleration of the suspended load due to the control force demand and the disturbance force (see Figure 4.4) is given by:

$$s^2 Z(s) = \frac{F_{demand}(s)}{m(1+sT_{force})} + \frac{F_{disturb}(s)}{m} \qquad \textbf{4.2}$$

The Laplace transfer function for the full closed-loop position controller is obtained by substituting Equation 4.1 into Equation 4.2. After rearranging and collecting terms (see Appendix C), the reference position transfer function is given by:

$$\frac{Z(s)}{Z_{ref}(s)} = \frac{k_{pos}(s+1/T_{err})(s+\omega_{int})^2}{s^6(mT_{force}) + s^5(k_{acc}+m+2\omega_{int}mT_{force}) + s^4(k_{vel}+2\omega_{int}(k_{acc}+m)+\omega_{int}^2 mT_{force}) + s^3(k_{pos}+\omega_{int}^2(k_{acc}+m)+\omega_{int}k_{vel}) + s^2(k_{pos}/T_{err})} \qquad \textbf{4.3}$$

and the disturbance force transfer function is given by:

$$\frac{Z(s)}{F_{disturb}(s)} = \frac{(1+sT_{force})(s+\omega_{int})^2}{s^5(mT_{force}) + s^4(k_{acc}+m+2\omega_{int}mT_{force}) + s^3(k_{vel}+2\omega_{int}(k_{acc}+m)+\omega_{int}^2 mT_{force}) + s^2(k_{pos}+\omega_{int}^2(k_{acc}+m)+\omega_{int}k_{vel}) + s(k_{pos}/T_{err})} \qquad \textbf{4.4}$$

The reference position transfer function has 6 poles and 3 zeros so the closed-loop position control system is a sixth-order system. However, since the guideway following algorithm passes frequencies below ω_{int}, the position feedback signal can be assumed

to be dc coupled. This results in the transfer function zeros due to the state integration filters moving to the origin of the *s*-plane, where they cancel with the poles at the origin. The closed-loop response is therefore effectively that of a fourth-order system, with two poles due to the sprung mass, one pole due to the position error integral action, and another pole is contributed by the force actuator. Furthermore, the high stiffness required of the position controller permits the use of a slow error integration time constant. The position controller can therefore be designed as a dominantly third-order system with a fourth pole located close to the origin due to the error integral action. If the force actuation time constant is sufficiently small, then the system reduces to a dominantly second-order system. However, since the electromagnet force actuation bandwidth is limited by cost and complexity considerations, the force actuation pole cannot be neglected.

Synthesis of the position control algorithm can be considerably simplified if the dominant response of the controller is that of a second-order system.[70] To permit this design approach, the position control system is reduced to a second-order system by assuming infinite force bandwidth, by neglecting error integral action, and by assuming that the suspension velocity and position are measured directly. After designing the state feedback gains for the reduced-order system, the constraints for the neglected terms are calculated to ensure an acceptable full closed-loop transfer function.

Since the guideway following algorithm determines the passenger ride characteristic, the detailed characteristic behaviour of the position controller transfer function is not critical. The primary requirements are that the position controller bandwidth is sufficiently high, and that the response is adequately damped. In practice, the high stiffness required for the force disturbance rejection ensures sufficient bandwidth, and the damping is an independent design factor.

The reduced-order position transfer function is obtained by substituting values of $T_{force} = 0$, $T_{err} = \infty$ and $\omega_{int} = 0$ into Equations 4.3 and 4.4. This substitution gives:

$$Z(s) = \frac{k_{pos}}{\left(s^2(k_{acc}+m) + s k_{vel} + k_{pos}\right)} Z_{ref}(s) + \frac{1}{\left(s^2(k_{acc}+m) + s k_{vel} + k_{pos}\right)} F_{disturb}(s) \quad \textbf{4.5}$$

The characteristic behaviour of this second-order transfer function can be conveniently expressed in terms of its undamped natural frequency, ω_n, and damping ratio, ζ. The standard form for a second-order transfer function and the location of its poles is given by:

$$\frac{1}{s^2/\omega_n^2 + 2\zeta s/\omega_n + 1} \qquad \textit{with poles at:} \qquad s = -\omega_n\zeta \pm \omega_n\sqrt{\zeta^2 - 1} \qquad \textbf{4.6}$$

The undamped natural frequency and damping ratio of the closed-loop position control transfer function (Equation 4.5) are thus given by:

$$\omega_n = \sqrt{\frac{k_{pos}}{k_{acc} + m}} \qquad \zeta = \frac{k_{vel}}{2\sqrt{(k_{acc} + m)k_{pos}}} \qquad \textbf{4.7}$$

4.4.2 Position, velocity and acceleration feedback gains

The most exacting requirement for the position controller is the rejection of disturbance forces. The controller must limit the transient deflection due to a force disturbance of 50% of the full load force, to half of the maximum suspension deviation (see Section 4.2).

The maximum total suspended load for the experimental electromagnet is 50 kg and its nominal operating air gap is 3 mm with an operational deflection of up to ±2 mm (see Table 3.1). Therefore, accommodation of a 50% load change, within half the operational air gap deflection, requires a suspension stiffness, k_{pos}, given by:

$$k_{pos} = 50\% \times 50 \text{ kg} \times 9.81 \text{ Nkg}^{-1} \div 1 \text{ mm} \approx 250 \text{ N/mm}$$

If k_{acc} is initially assumed to be zero, k_{pos} = 250 N/mm and m = 15 kg, then the undamped natural frequency of the position controller (see Equation 4.7) is 20 Hz, while for m = 50 kg, the undamped natural frequency falls to 11 Hz. The use of acceleration feedback can reduce this variation in natural frequency due to a load change by providing 'virtual mass'. Acceleration feedback is functionally equivalent to force feedback, so it effectively increases the force bandwidth and enhances linearity and stability. However, due to the constrained achievable force bandwidth (see Chapter 3), k_{acc} must be kept to a sensible minimum. The breakpoint for the effectiveness of acceleration feedback in ameliorating the impact of load changes occurs when k_{acc} = minimum mass, so this is proposed as an acceptable compromise. With k_{acc} = 15 kg, the undamped natural frequency is reduced to 15 Hz and 10 Hz at no load

and full load respectively. The acceleration feedback gain is effectively equivalent to a force feedback gain of 1 at the minimum load.

Since the underlying electromagnetic force actuator is open-loop unstable, a well damped response is considered prudent in order to produce a robust suspension which is insensitive to force actuation errors by the electromagnet force controller. In addition, since the operational air gap range is limited, overshoot of the position response is undesirable. Therefore, a worst case damping ratio given by the critical damping ratio[71] of 0.707 is required. To allow a margin for feedback gain deviations due to transducer errors of up to ±25%, a minimum nominal value for ζ of 0.8 is required. This requires a velocity feedback gain (see Equation 4.7) of k_{vel} = 6500 N/(m/s), which gives a nominal damping ratio of 0.8 and 1.2 at full and minimum load respectively. In practice, the minimum damping ratio will be higher if the suspended load is a passenger. This is because the passenger's mass will not be rigidly coupled to the vehicle at the natural frequency of the position controller.

4.4.3 Force actuation bandwidth

Having designed the response of the reduced-order position controller, the required force actuation bandwidth is now determined. The transfer function for the position control system, neglecting only the low frequency components due to the state integration filters and position error integral action, is obtained by substituting values of $T_{err} = \infty$ and $\omega_{int} = 0$ into Equation 4.3. This substitution yields:

$$\frac{Z(s)}{Z_{ref}(s)} = \frac{k_{pos}}{s^3 m T_{force} + s^2 (m + k_{acc}) + s k_{vel} + k_{pos}} \qquad \textbf{4.8}$$

Table 4.2 lists the location of the closed-loop poles for minimum and maximum suspended masses over a range of force actuation bandwidths. The location of the poles is strongly influenced by both the force actuation bandwidth and the suspended mass, and the damping ratio relates to the complex conjugate pole pair or the dominant pair of real poles. As expected, the table shows that the damping ratio falls sharply once the force actuation bandwidth approaches that of the reduced-order position control system. To ensure an adequately damped response, and to allow a margin for transducer errors, a force actuation bandwidth of about 50 Hz is required, which is equivalent to a force time constant, T_{force} = 3.2 ms.

Table 4.2 Variation of closed-loop poles with force bandwidth

Force bandwidth		**Closed-loop poles (m=15kg)**		**Closed-loop poles (m=50kg)**	
Hz	**rad/s**	**Location**	ζ	**Location**	ζ
∞	∞	-∞, -167, -50	1.19	-∞, -50 ±j37	0.80
1000	6283	-12347, -170, -50	1.19	-8067, -50 ±j37	0.80
100	628	-993, -214, -49	1.28	-708, -55 ±j38	0.82
50	**314**	**-290 ±j155, -48**	**0.88**	**-284, -62 ±j41**	**0.83**
40	251	-227 ±j188, -48	0.77	-190, -69 ±j44	0.84
30	188	-165 ±j197, -47	0.64	-88, -78 ±j67	0.75
20	125	-102 ±j186, -46	0.48	-63, -50 ±j86	0.50

4.4.4 Position error integral time constant

The final feedback gain factor to be determined is the time constant for the position error integral action. Since the stiffness of the controller is high, the functional requirement for the integral action, that of eliminating steady-state position errors, can be performed quite slowly. This enables the closed-loop pole due to the integral action to be placed close to the origin of the *s*-plane where it has negligible impact on the other system poles. The slowest closed-loop pole is located at s = -48 (see the highlighted row in Table 4.2), and has a time constant of 21 ms. Therefore, a value for the integral action time constant, T_{err}, of 1 second will cause negligible disturbance of the other closed-loop poles. Position error integral action is thus introduced without impairing the dynamic response or damping of the position controller.

4.4.5 Guideway following algorithm

The guideway following algorithm is required to limit the acceleration due to a ±1 mm step change in track height to about ±0.2 m/s^2 (see Section 4.2). Since acceleration is the second derivative of position, the proposed second-order low-pass filter can be

designed to limit the acceleration to any desired level for a given track step size. The Laplace transform of such a filter, with a damping ratio of 1, is given by:

$$Guideway\_filter(s) = \frac{\omega_{follow}}{\left(s + \omega_{follow}\right)^2} \qquad \textbf{4.9}$$

where ω_{follow} is the guideway following filter corner frequency. For a step input of amplitude Δpos, the acceleration of the filter response is given by:

$$Acc(s) = s^2 \frac{\Delta pos}{s} \frac{\omega_{follow}}{\left(s + \omega_{follow}\right)^2} = \Delta pos \frac{s\,\omega_{follow}}{\left(s + \omega_{follow}\right)^2} \qquad \textbf{4.10}$$

The corresponding acceleration response in the time domain is given by:

$$acc(t) = \Delta pos\ \omega_{follow}^2\ e^{-\omega_{follow} t}\left(1 - \omega_{follow} t\right) \qquad \textbf{4.11}$$

Inspection of this time domain response reveals that the peak acceleration occurs at time t=0. The guideway filter time constant required to limit the acceleration to acc_{max} is thus obtained by setting t=0 and $acc(t)$=acc_{max}. After rearranging, this gives:

$$\omega_{follow} = \sqrt{\frac{acc_{\max}}{\Delta pos}} \qquad \textbf{4.12}$$

Therefore, to accommodate a track step size of ±1 mm, with a peak acceleration of the filter output of ±0.2 m/s^2, a low pass filter, with two poles at s = 10,10 is required.

However, the poles of the closed-loop position controller transfer function limit the initial acceleration of the suspension to zero. Since an exact numerical solution for the maximum acceleration of the full suspension control system is unduly complicated, the two pole guideway following filter is simulated along with a representative pole from the position controller transfer function. Examination of Table 4.2 shows that the position controller can be effectively modelled for this purpose by a single pole at s = 48. The simulation results show a peak acceleration for three poles at s = 10,10,48 of 0.05 m/s^2, which is much lower than that required. The guideway following filter poles are therefore moved so that s = 25,25,48 where they produce a peak acceleration of 0.21 m/s^2. The bandwidth of the guideway following filter, ω_{follow} is thus set to 25 rad/s, and the overall track/suspension position response is approximated by three poles at s = 25,25,48.

To prevent the suspension system from exciting track vibrations, the natural frequency of the track must be above the track following frequency of 4 Hz.

4.4.6 State integration filters

The position controller synthesis has so far assumed dc coupled feedback signals for acceleration, velocity and position. However, since the state integration is augmented with high-pass filtering, it is necessary to determine the constraints that must be imposed upon the filter corner frequency in order to limit the dislocation of the closed-loop poles by the filters.

Neglecting the high frequency component due to the force actuation time constant, the transfer function of the closed-loop position control system is obtained by substituting the value $T_{force} = 0$ into Equation 4.3. This substitution gives:

$$\frac{Z(s)}{Z_{ref}(s)} = \frac{k_{pos}\,\left(s + 1/T_{err}\right)\,\left(s + \omega_{int}\right)^2}{s^5\left(k_{acc}+m\right) + s^4\left(k_{vel} + 2\omega_{int}(k_{acc}+m)\right) + s^3\left(k_{pos} + \omega_{int}^2(k_{acc}+m) + \omega_{int}k_{vel}\right) + s^2\left(k_{pos}/T_{err}\right)} \qquad \textbf{4.13}$$

The integration filter corner frequency, ω_{int}, is present in the characteristic polynomial as a factor in the s^4 and s^3 terms. These terms are therefore used to determine constraints on ω_{int} such that the characteristic polynomial is not materially altered by the integration filters. The first term produces the constraint given by:

$$2\omega_{int}(k_{acc}+m) \ll k_{vel} \qquad \therefore \qquad \omega_{int} \ll \frac{k_{vel}}{2(k_{acc}+m)} \qquad \textbf{4.14}$$

The second constraint is simplified using the first constraint and is given by:

$$\omega_{int}\left[\omega_{int}(k_{acc}+m) + k_{vel}\right] \ll k_{pos} \qquad \therefore \qquad \omega_{int} \ll \frac{k_{pos}}{k_{vel}} \qquad \textbf{4.15}$$

For the controller feedback gains determined earlier (see Table 4.3), the filter corner frequency, ω_{int}, must be much lower than 38 rad/s.

An additional constraining factor is due to the bandwidth of the guideway following algorithm. Since this provides a relative position signal at frequencies below 25 rad/s (see previous section), the state integration filters must pass frequencies above 25 rad/s.

Therefore, ω_{int} must be much less than 25 rad/s in order to be able to assume that the position feedback is dc coupled, and hence assume that the state integration filter zeros cancel the poles at the origin of the closed-loop transfer function (see Equation 4.13).

The low frequency limit that can be achieved in practice is determined by the system implementation (see Chapter 6). The limiting factors include the hysteresis, non-linearity, and resolution of the accelerometer and its analogue-to-digital converter, along with the numerical techniques and precision used to implement the filters. Since achieving a very low frequency response is costly, an acceptable performance and cost trade-off is required.

Experimentation with a sensor which met the other system requirements demonstrated that a low frequency cut-off of 0.6 rad/s is achievable. With ω_{int} = 0.6 rad/s, the two state integration filters reduce the position signal amplitude by a total of 5-7.5% at 15-25 rad/s. Due to offsets present within the analogue parts of the experimental system, two additional high-pass filters are applied to the measured acceleration signal before it can be used. For frequencies of 15-25 rad/s, this gives rise to a total loss of position signal amplitude of 10-15%. An overshoot of approximately this size is therefore expected on the closed-loop suspension position response to a track step. The size of the overshoot is increased further by the velocity feedback signal. If desired, it may be possible to compensate for most of the position signal gain loss by increasing the gain of the air gap signal to match the low frequency gain loss of the position signal.

4.4.7 Suspension controller design specification

By adhering to the constraints identified in the preceding section for the state integration filter bandwidth, the closed-loop transfer functions for the position controller (see Equations 4.3 and 4.4) can be expressed more simply by:

$$\frac{Z(s)}{Z_{ref}(s)} = \frac{k_{pos}\ (s + 1/T_{err})}{s^4(mT_{force}) + s^3(k_{acc} + m) + s^2 k_{vel} + s k_{pos} + k_{pos}/T_{err}} \qquad \textbf{4.16}$$

and

$$\frac{Z(s)}{F_{disturb}(s)} = \frac{s\ (1 + sT_{force})}{s^4(m\,T_{force}) + s^3(k_{acc} + m) + s^2 k_{vel} + s\,k_{pos} + k_{pos}/T_{err}} \qquad \textbf{4.17}$$

The closed-loop suspension/track position transfer function is obtained by augmenting Equation 4.16 with Equation 4.9. This gives:

$$\frac{Z(s)}{P(s)} = \frac{\omega_{follow}^2\ k_{pos}\ (s + 1/T_{err})}{(s + \omega_{follow})^2 \left[s^4(m\,T_{force}) + s^3(k_{acc} + m) + s^2 k_{vel} + s\,k_{pos} + k_{pos}/T_{err}\right]} \qquad \textbf{4.18}$$

This is dominated by the guideway following filter and can therefore be approximated by Equation 4.9 alone, giving:

$$\frac{Z(s)}{P(s)} \approx \frac{\omega_{follow}^2}{(s + \omega_{follow})^2} \qquad \textbf{4.19}$$

The suspension control system parameters designed earlier are summarised in Table 4.3, and the closed-loop poles and zeros that these produce (see Equation 4.18) are listed in Table 4.4.

Table 4.3 Suspension control system parameters

Parameter	Name	Value
Stiffness	k_{pos}	250 N/mm
Damping	k_{vel}	6.5 N/(mm/s)
Virtual mass	k_{acc}	15 kg
Error integral time constant	T_{err}	1 s
Force actuation time constant	T_{force}	3.2 ms
State integration filter frequency	ω_{int}	0.6 rad/s
Guideway following frequency	ω_{follow}	25 rad/s

Table 4.4 Closed-loop suspension system zeros and poles

Mass	Position Controller			Guideway Filter
	Zero	**Poles**	$\zeta_{\text{complex.poles}}$	**Poles**
15 kg	-1	-290 ±j157, -48, 0	0.88	-25, -25
50 kg	-1	-281, -63 ±j40, 0	0.84	-25, -25

4.5 Lateral guidance

In order to reduce the complexity of the implementation of the experimental vehicle and single electromagnet rig, provision has not been made for lateral force control. The problem of controlling the lateral force is minor compared with that of controlling the lift force, since the lateral behaviour of the electromagnetic suspension is open-loop stable.

Without active control, the suspension experiences lateral stiffness due to the geometry of the shear flux between the electromagnet and track poles. However there is negligible lateral damping so a brief analysis to ascertain the lateral stiffness and natural frequency of the lateral motion is considered prudent.

For lateral offsets of up to 2/3 of the electromagnet pole width, the lateral force (see Equation 2.10) is approximated by:

$$F_{lateral} = F_{magnet} \frac{2c}{\pi p} \tan^{-1}\left(\frac{y}{c}\right) \qquad \textbf{4.20}$$

where F_{magnet} is the gross electromagnet force, c is the air gap, y is the lateral offset, and p is the pole width. The lateral stiffness can therefore be approximated by:

$$k_{lateral} = \frac{F_{lateral}}{y} = m_t a_g \frac{2c}{\pi p y} \tan^{-1}\left(\frac{y}{c}\right) \qquad \textbf{4.21}$$

where m_t is the total suspended mass and a_g is the acceleration due to gravity. Although this is a nonlinear function, it can be linearised for small lateral offsets by:

$$k_{lateral} \approx \frac{2m_t a_g}{\pi p} \qquad for \qquad y<c \tag{4.22}$$

The laterally sprung mass is therefore assumed to have a dominantly second-order response, with the natural undamped angular frequency (see Section 4.4.1) of the lateral motion approximately given by:

$$\omega_n \approx \sqrt{\frac{2m_t a_g}{m_c \pi p}} \tag{4.23}$$

where m_c is the effective, rigidly coupled suspended mass.

For any suspension load which is rigidly coupled to the electromagnet, the model predicts a natural undamped frequency of 4 Hz. However, with a human passenger load, the natural frequency of the human body lateral coupling is likely to be below 4 Hz, and so the natural undamped frequency of the lateral motion could be as high as 7 Hz. In practice, it is likely to lie somewhere in the range of 4 Hz to 7 Hz. The natural lateral suspension frequency is thus similar to that designed for the vertical track following algorithm. A beneficial side effect of human body to vehicle coupling for the experimental systems is that it provides a degree of lateral damping.

The presence of the air gap in the lateral force model (see Equation 4.20) presents the interesting possibility of providing lateral damping by controlling the lateral force through modulation of the air gap. Clearly, such a technique would impose a disturbance on the vertical motion, but it would provide lateral damping without the need for additional electromagnets. However, since no problems have been experienced with regard to lateral motion oscillations, this technique has not been investigated.

4.6 Performance of the experimental mode suspension

In order to validate the theoretical basis of the design of the proposed suspension control system, the system was simulated and various step responses were obtained and examined. An experimental single electromagnet suspension system was then developed (see Chapter 6) and the experimental system was tested by comparing a number of simulated and experimental responses.

The control system was simulated using the Advanced Continuous Simulation Language (ACSL)[72] which provides high level simulation constructs and has powerful signal monitoring capabilities. The model of the suspension control system is listed in Appendix C and incorporates a discrete-time suspension controller with analogue-digital conversion quantisation, and continuous-time models of the electromagnet and control system transducers.

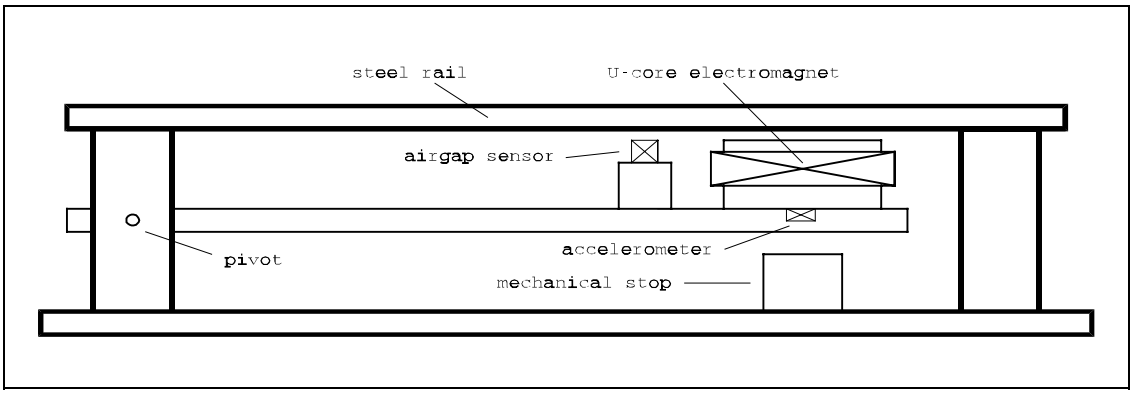

Figure 4.5 Single electromagnet suspension experimental rig

Figure 4.5 (Figure 3.7 repeated) shows the physical arrangement of the experimental single electromagnet test rig in which the long pivoted beam allows the electromagnet and sensors to move with negligible stiffness and damping in the vertical direction. The control system was designed using the suspension configuration shown in Figure 4.4 with the parameters defined in Table 4.3.

Step changes in track height are simulated by injecting an offset into the track profile calculation. The full bandwidth response of the position controller is tested by bypassing the guideway following algorithm, thus effectively setting the guideway following filter bandwidth to infinity. This results in the position error signal consisting solely of the air gap signal with no contribution from the absolute position signal. After testing the position controller response, the system is reconfigured with the correct guideway following filter to verify that the suspension meets the required ride comfort specification.

4.6.1 Position controller

Figure 4.6 and Figure 4.7 show the simulated and experimental position controller responses respectively, for a 1 mm step size, and a suspended mass of 15 kg. Figure 4.8 and Figure 4.9 show the respective responses for a suspended mass of 45 kg.

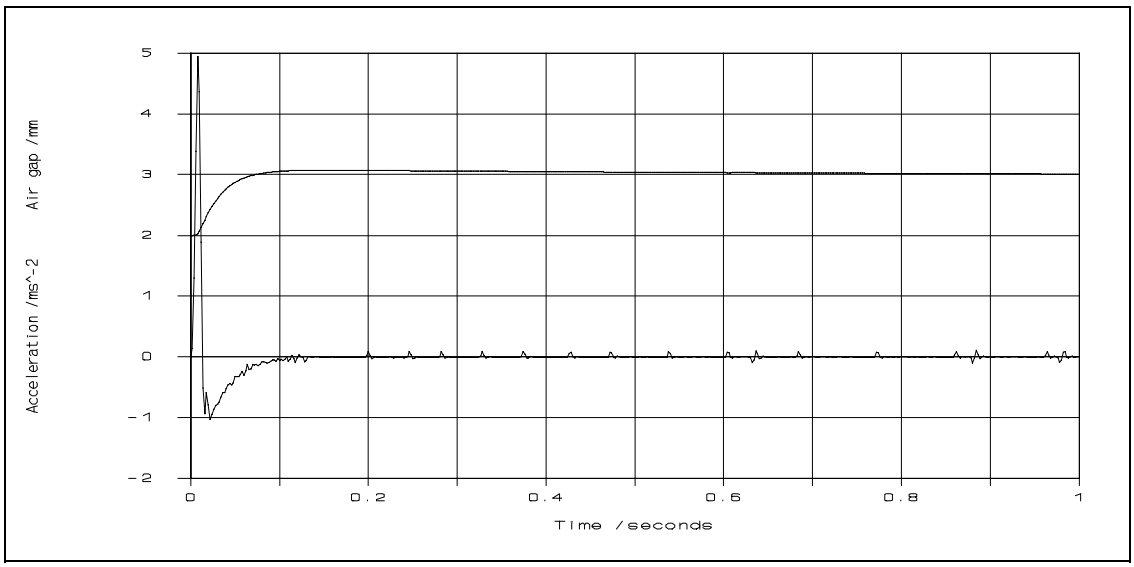

Figure 4.6 Simulated suspension response to a 1 mm air gap reference step (ω_{follow} = ∞ rad/s, m = 15 kg)

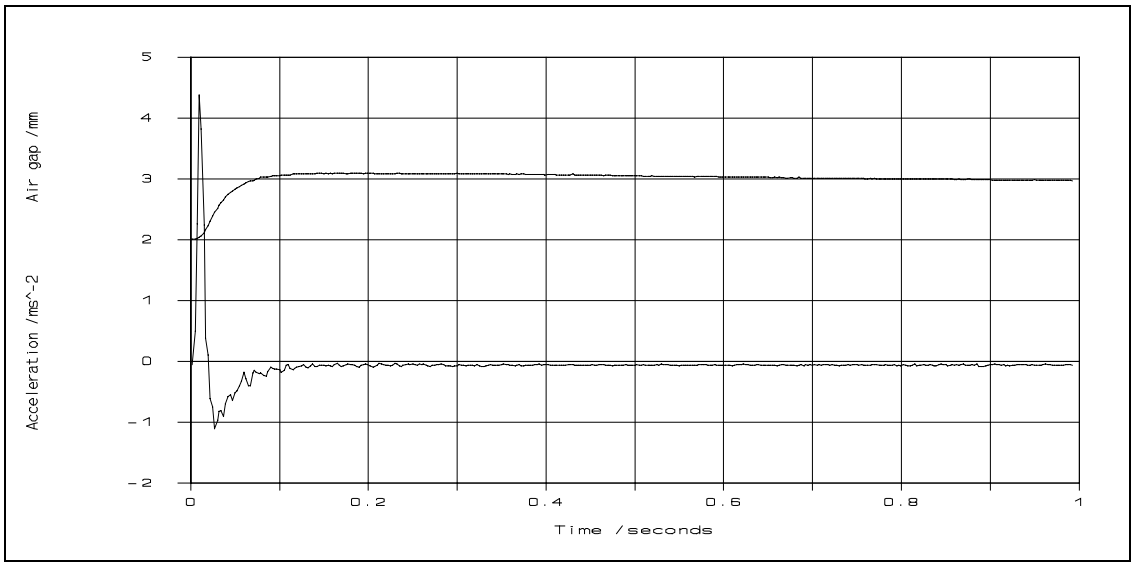

Figure 4.7 Experimental suspension response to a 1 mm air gap reference step (ω_{follow} = ∞ rad/s, m = 15 kg)

The air gap responses are well damped, with a small, very low frequency overshoot. The 7% overshoot on the simulated responses is due solely to the high-pass filtering of the velocity feedback signal. This is augmented on the experimental responses by an additional 5% overshoot due to the force actuation error as the electromagnet operating point changes with the air gap. The experimental response for the 45 kg suspended mass has a further 5% overshoot (bringing its total to 17%) which can be attributed to the damping ratio being slightly below the critical damping ratio.

The sharp peaks for the acceleration responses are caused by current slew rate limiting in the electromagnet current controller. This occurs because the force slew rate is

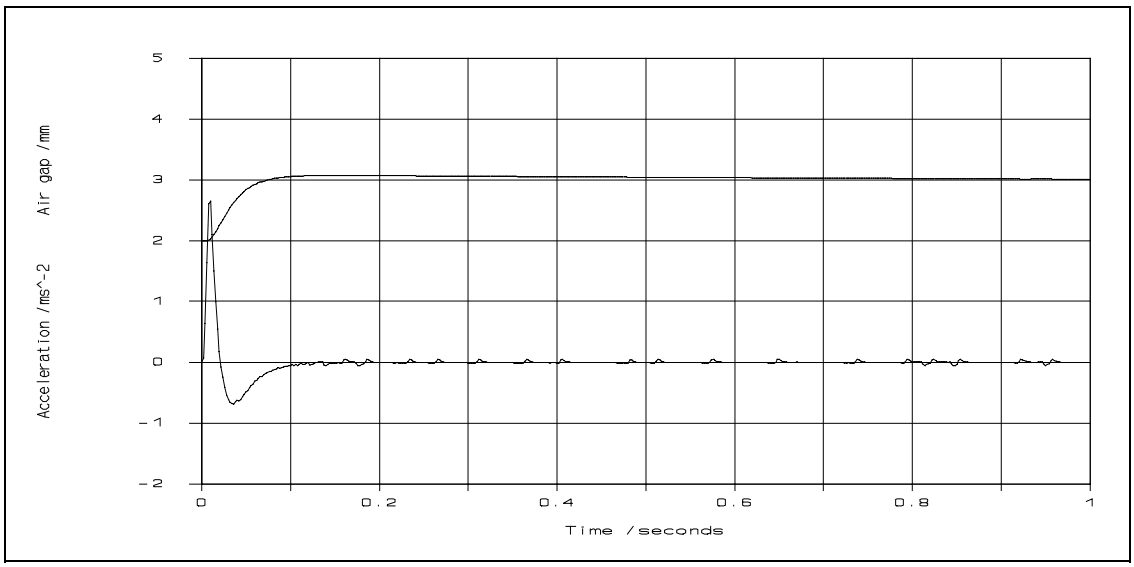

Figure 4.8 Simulated suspension response to a 1 mm air gap reference step (ω_{follow} = ∞ rad/s, m = 45 kg)

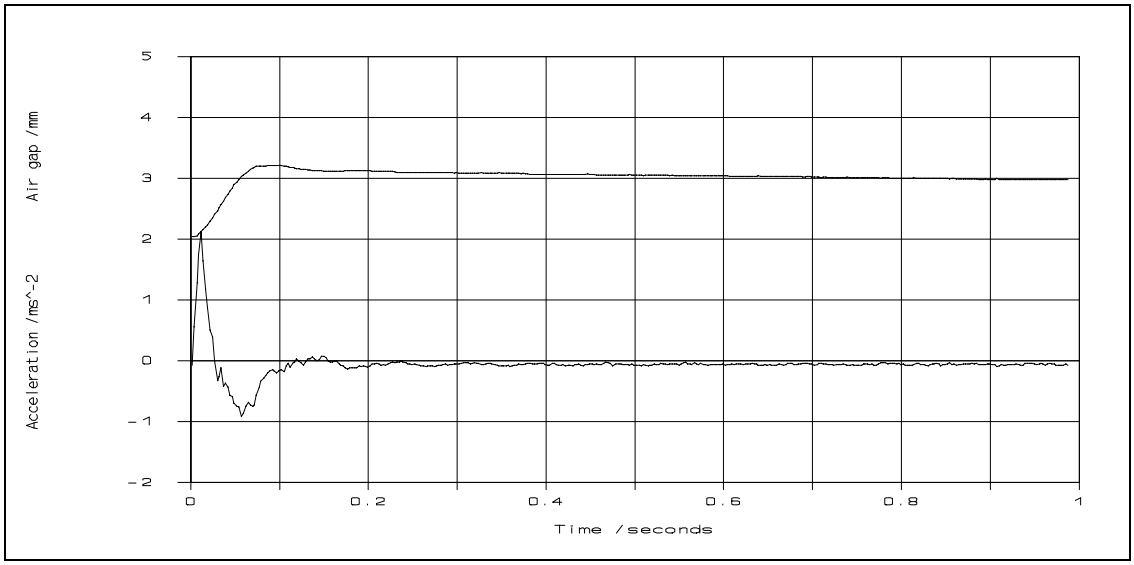

Figure 4.9 Experimental suspension response to a 1 mm air gap reference step (ω_{follow} = ∞ rad/s, m = 45 kg)

designed for comfortable passenger acceleration levels rather than the high levels experienced during these tests. The time to the acceleration peak is approximately 9 ms for both the experimental and simulated responses. The peak acceleration amplitudes of the experimental responses are 10-20% lower than the simulated responses which suggests that the bandwidth or force slew rate of the experimental system is slightly lower than the design target.

The low amplitude oscillation superimposed on the transient experimental acceleration responses (up to time = 150 ms) is partly due to the current slew rate limiting, but is mostly due to the force pulse causing the experimental rig to vibrate. The natural

frequency of the rig is about 60 Hz and the oscillation decays rapidly. However, the natural frequency can be reduced down to about 10 Hz by using flexible rubber mountings. As expected, at rig natural frequencies close to that of the position controller (approximately 10-15 Hz), the rig could be excited with a step position reference to produce continuous steady-state oscillation. The rig oscillation presented no electromagnet stability problems, but it is obviously unacceptable. Setting the rig natural frequency to double that of the air gap controller is sufficient to cause any oscillation to decay rapidly.

The acceleration ripple which is apparent in the steady state on both the experimental and simulated responses is due to limit cycling[73] of the air gap. The period and magnitude of the limit cycle is primarily a function of the air gap measurement resolution and hysteresis, and conversion quantisation, but it is also affected by the controller sampling period and the electromagnet operating point. The amplitude of the limit cycles for the experimental responses is approximately one third that of the simulated responses. This is attributed to measurement noise in the experimental system increasing the effective analogue to digital conversion resolution.[74]

The results discussed above give confidence in the linearity and bandwidth of the electromagnet force actuator developed in Chapter 3. However, additional responses were obtained to test the performance of the suspension over its full operational envelope. Figure 4.10 presents the results of a test in which three step responses were obtained, each stepping up and then down by 1 mm, from initial air gaps of 1.5, 2.5 and 3.5 mm. The consistent responses demonstrate the fact that the electromagnet force actuator provides an acceptably linear response over the full operational air gap range.

The disturbance force rejection requirement of the suspension is tested by rapidly applying and removing a 15 kg load. This produces a peak air gap deflection of ±0.73 mm, whilst the expected theoretical deflection is ±0.6 mm. The 20% discrepancy is attributed to sensor and force actuation errors. The air gap deflection recovers by 90% within 2 seconds of the application of the force disturbance, and is subsequently eliminated.

The overall correspondence between the steady-state and dynamic characteristics of the simulated and experimental responses is good, and the air gap response is well damped. Further position controller test results, including disturbance force rejection and the frequency domain response are presented in Chapter 5 for the multi-electromagnet vehicle.

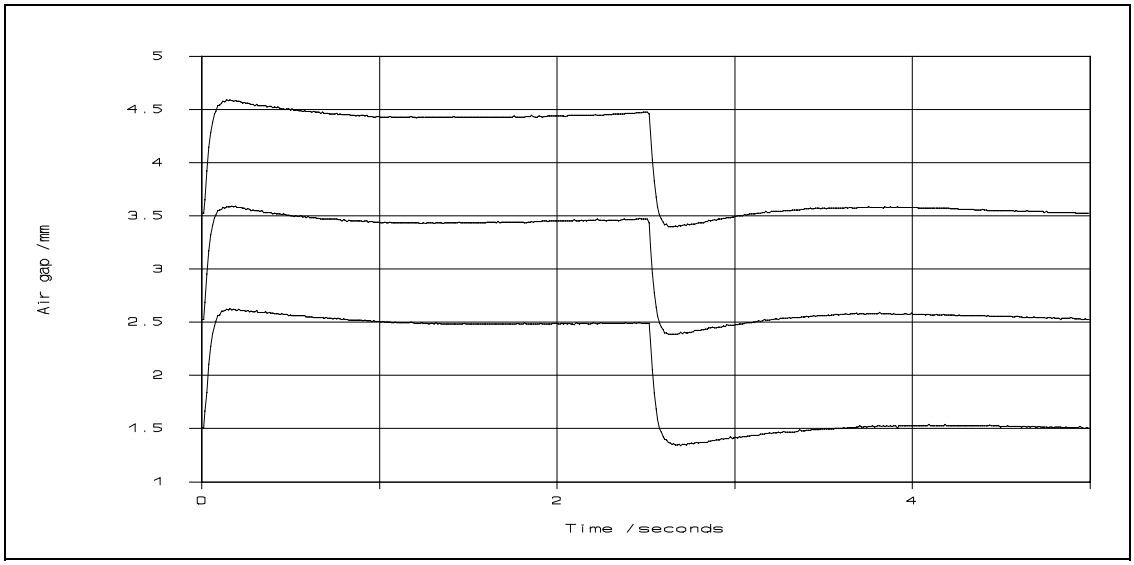

Figure 4.10 Experimental suspension responses to three 1 mm air gap reference steps ($\omega_{follow} = \infty$ rad/s, m = 30 kg)

4.6.2 Full suspension system

The ability of the suspension control system to meet the required ride comfort level is now examined. Since the reaction rail of the experimental electromagnet rig cannot be moved, track steps are simulated by injecting a step disturbance into the track position calculation before the guideway following algorithm. Figure 4.11 and Figure 4.12 illustrate the simulated and experimental responses respectively, for a (simulated) 1 mm step in track height, with a suspended mass of 15 kg. Figure 4.13 and Figure 4.14 show the respective responses for a suspended mass of 45 kg.

The peak acceleration of the simulated responses is 0.21 m/s^2 which is very close to the design value of 0.21 m/s^2. The peak accelerations of the experimental responses are 0.28 and 0.30 m/s^2 for the 15 and 45 kg suspended masses respectively, which are 27% and 36% above the design target. Since the peak acceleration is quite sensitive to the location of the position controller poles, the experimental acceleration levels are attributed to errors in the assumed position controller poles. These errors arise due to inaccuracies in the sensor measurements in general, and the electromagnet force actuator in particular. The response for the 45 kg mass shows evidence of a low amplitude oscillation of the experimental rig at a frequency of about 5 Hz. Both experimental acceleration responses are however, well within the ISO ride comfort specification of 0.4 m/s^2, and a consistent response is achieved even when the suspended mass is tripled. The sensitivity of the acceleration response to the location of the position controller poles can be ameliorated through the use of a more complex guideway following

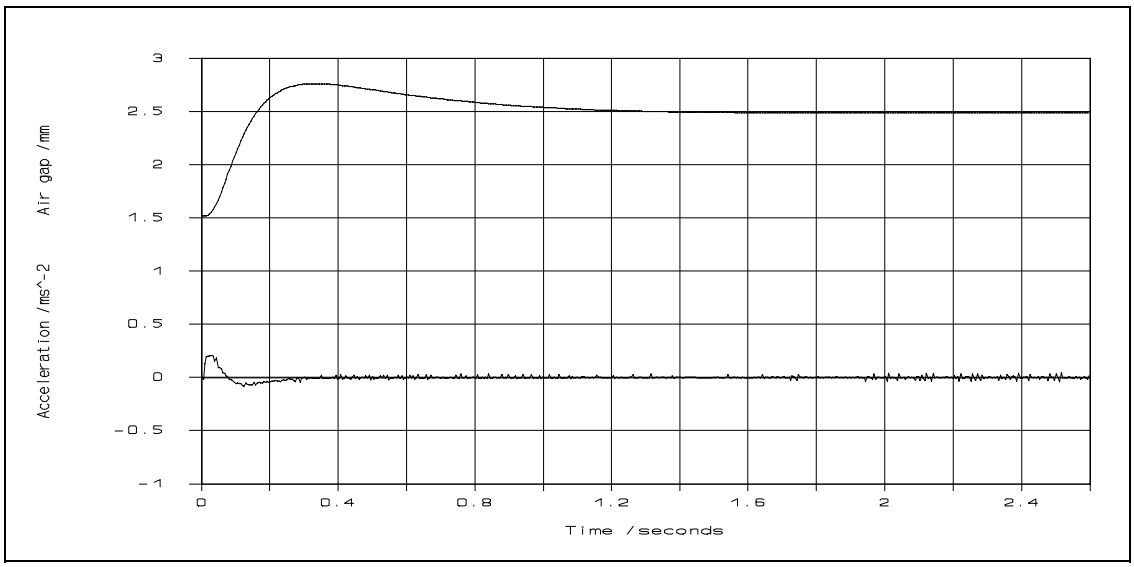

Figure 4.11 Simulated suspension response to a 1 mm simulated track step (m = 15 kg)

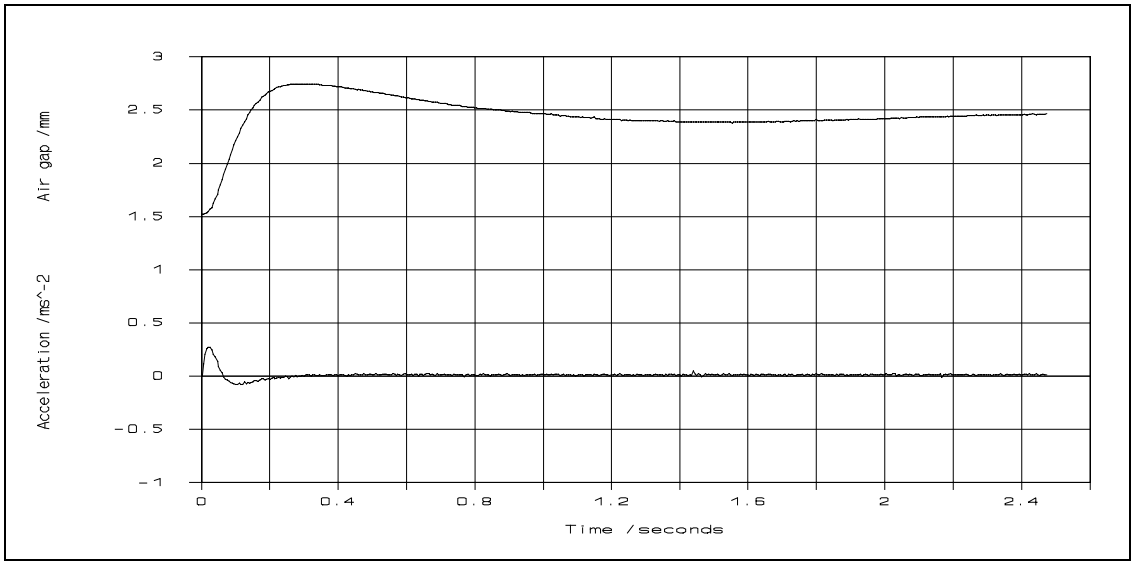

Figure 4.12 Experimental suspension response to a 1 mm simulated track step (m = 15 kg)

algorithm, for example, by using a third-order filter.

The low frequency overshoot on the air gap step responses for both the simulated and the experimental results is around 23%. The overshoot is dominantly due to the state integration filters which reduce the amplitude of the position and velocity feedback signals at low frequencies. The 23% overshoot is close to that anticipated with a 10-15% contribution from the position signal (see Section 4.4.6) plus a 7% contribution from the velocity signal which was observed in the position controller test. For the experimental system, this overshoot is considered acceptable.

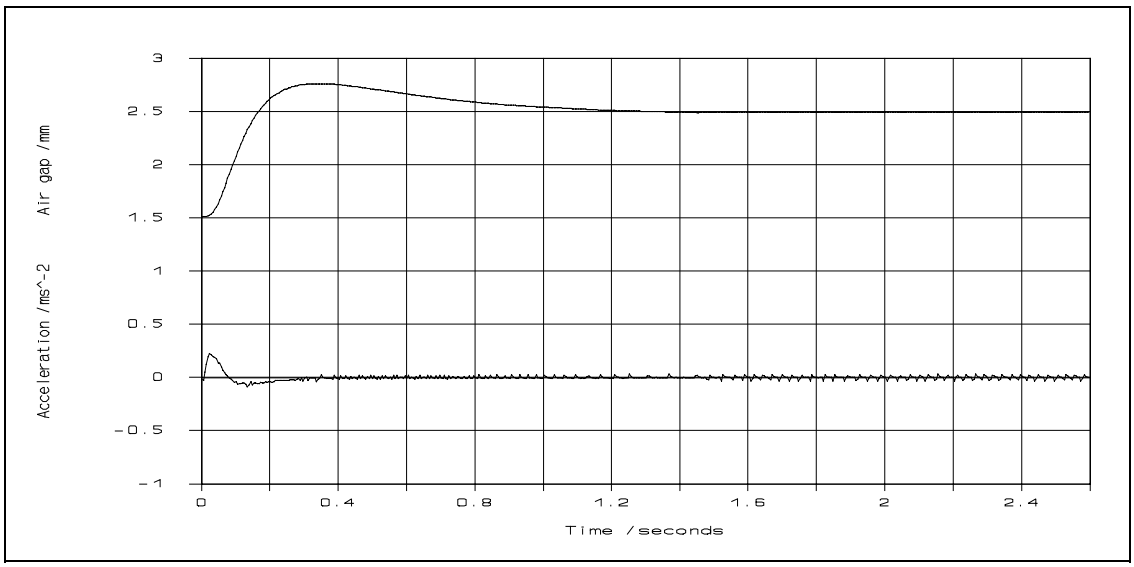

Figure 4.13 Simulated suspension response to a 1 mm simulated track step (m = 45 kg)

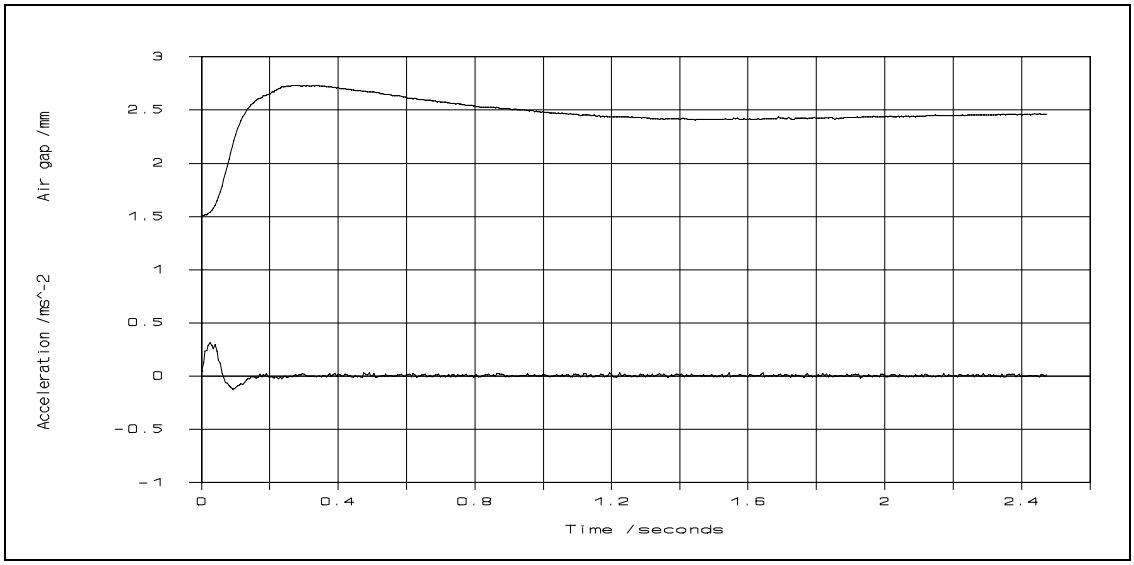

Figure 4.14 Experimental suspension response to a 1 mm simulated track step (m = 45 kg)

The track step response test described above is in fact rather harsh, since a step change in track height for a moving electromagnet is transformed to a ramp change as the electromagnet passes by the step. Since full-scale suspension magnets are quite long[75] (typically 1 m, for speeds of 0-25 m/s) this transformation adds a further filter to the system, which can be approximated by a first order lag with a pole frequency of 0-25 rad/s (speed divided by electromagnet length). A real track step would therefore produce a lower peak acceleration than the simulated track steps.

4.7 Conclusions

A novel suspension control scheme has been proposed, developed, and tested, which permits the conflicting requirements of disturbance force rejection and guideway following to be designed independently. Simulated and experimental test results show that the system meets the functional requirements, and that the response is stable and well damped.

For a full-scale system, it may be desirable to reduce the air gap overshoot associated with step changes in the track height. Further research investigating higher performance accelerometers, more complex state integration filters, and air gap gain compensation should permit a reduction in the air gap overshoot.

The development of a sophisticated guideway following algorithm suitable for use on guideways with gradients is an area that requires further research. The use of matched-filter techniques is considered to present potential improvements over low-pass filtering. This research could be performed very largely through simulation studies.

Having established the validity of the proposed suspension control system, it is now ready to be applied to the suspension control of the experimental multi-electromagnet vehicle.